ISTITUTO NAZIONALE FISICA NUCLEARE

INFN/TC - 86/11
15 luglio 1986

D. Chiocca and A. Massarotti:

T.E. MODES IN WAVEGUIDES WITH PARALLELOGRAM CROSS-SECTION

Servizio Riproduzione della
Sezione di Trieste dell'INFN

T.E. MODES IN WAVEGUIDES WITH PARALLELOGRAM CROSS-SECTION

D. Chiocca
Dipartimento di Fisica
Università di Trieste

A. Massarotti
Dipartimento di Fisica
Università di Trieste
e
Sezione I.N.F.N. di Trieste

ABSTRACT: this paper deals with the TE modes of propagation in parallelogram-shaped waveguides. In particular, some theoretical considerations suggest that the dominant mode is at a lower frequency than that considered, for some parallelograms, in the current literature. This fact, tested through an experimental measure and a numerical simulation, has been found true.

INTRODUCTION

Suppose we have a waveguide, uniform in z direction, in which the modes of propagation vary as $\exp(j\omega t-\beta z)$.

Assume the metallic surfaces are made of perfect conductor and the guide is filled with isotropic ideal dieletric.

The expression governing the behaviour of the electromagnetic fields in this type of waveguide is the well known Helmoltz equation

$$(1) \qquad (\nabla_t^2 + k_c^2)\varphi = 0$$

where φ represents either E_z or H_z for TM and TE modes respectively, while k_c is the cutoff wave number and ∇_t^2 is the transverse laplacian operator.

Representing with k the free-space wave number, this quantity is related with k_c and β through the formula

$$(2) \qquad k_c^2 = k^2 + \beta^2$$

where $k^2 = \omega^2 \varepsilon \mu$, and μ and ε are respectively the permeability and permittivity of the dielectric.

To properly determine a solution of (1) it is necessary to give the correct boundary conditions, i.e.

$$(3) \qquad \varphi = 0 \qquad \text{at the conducting surfaces}$$

in the case of TM modes; or

$$(4) \qquad \partial\varphi/\partial n = 0 \qquad \text{at the conducting surfaces}$$

in the case of TE modes.

The latter condition, which in this work we are more interested to, is the more complex to handle, as we shall see.

Having solved (1) for φ and k_c, the other fields components are obtained with simple operations of derivation.

For TE modes we have

$$E_t = j\omega\mu\, \hat{z} \times \nabla_t \varphi / k_c^2 \qquad \text{and} \qquad H_t = -\beta\, \nabla_t \varphi / k_c^2$$

if $\hat{z}$ is the unit vector directed along the z-axis.

THEORY AND EXPERIMENTAL RESULTS

The literature on this topic deals only with particular cross-sections where the solution is available in terms of very elementary functions [1].

Solutions are known for the rhomb (fig. 1) with an acute angle of 60° [2], which one can think derived from the equilateral triangle [3], and for the parallelogram (fig. 2) with a base twice as the height and an acute angle of 45° [4], which can be considered as derived from the isosceles triangle with a right angle [5].

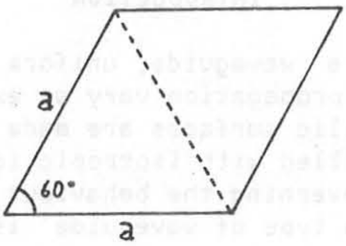

Fig. 1

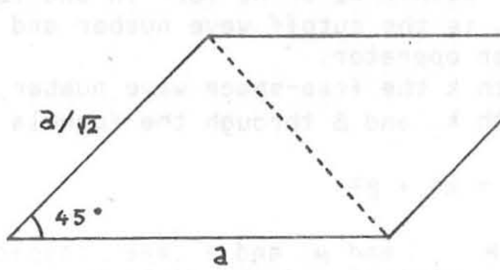

Fig. 2

In the case of the parallelogram is considered as the dominant TE mode the following:

(5) $$H_z = H_o \left(\cos(\pi x/b) + \cos(\pi y/b) \right)$$

(6) $$\lambda_c = 2b$$

where λ_c is the cutoff wavelenght.

Nevertheless the following theoretical considerations seem negate the fact that (5) and (6) really represent the dominant mode.

In fact an examination of the distribution of the transverse electric field (fig. 3a), suggests that the same field distribution could be obtained exciting in the TE_{01} mode a rectangular waveguide with sides 2b and $\sqrt{2}$ b (fig. 3b), and then shaping the cross section, by a parallel displacement of the top of the guide, in order to obtain a parallelogram as in fig. 3a. In this case the cut-off wavelenght is changed from $2\sqrt{2}$ b to 2b.

If we now excite the TE_{10} (dominant) mode in the rectangular guide so that λ_c = 4b and modify the cross section in the same way, the electromagnetic field distribution, for continuity reasons, must modify only as much is necessary to satisfy the new boundary conditions.

That is, because the main characteristic of this mode must remain unchanged, then the vertical component E_y of the electric field on the cross section of the waveguide must not undergo any change of sign. In the previous case, in fact, E_x did not change sign. Then it is expected an increase of the cut-off wavelenght.

Effectively this mode is the dominant one and then has the largest cut-off wavelenght. It is not considered in the known literature and till now the field equations are not known in terms of elementary functions.

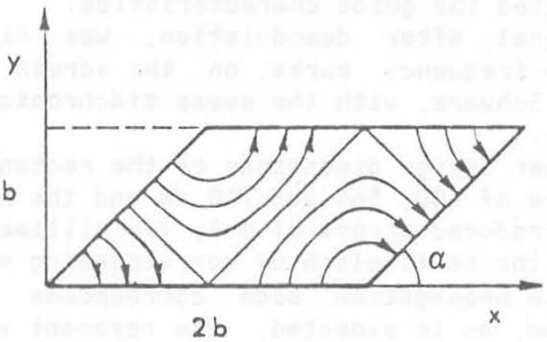

Fig. 3a - Transverse electric field pattern (TE_{01}) of the parallelogram waveguide with α=45°, obtained shaping the rectangular guide as indicated. The cut-off wavelenght is λ_c=2b.

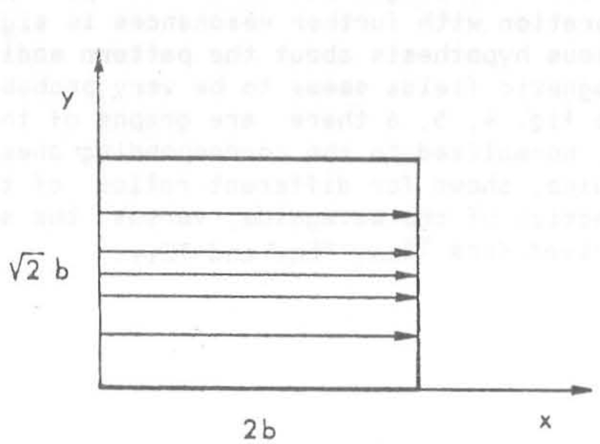

Fig. 3b - Transverse electric field pattern of the imperturbated rectangular guide excited in the TE_{01} mode. The cut-off wavelenght is $\lambda_c=2b\sqrt{2}$.

A piece of brass waveguide has been built to verify the correctness of the previsions. Some hinges, which allow the rectangular cross section to be changed into the parallelogram cross section, changing the acute angle α down to 30°, have been put along the corners of the guide.

The two ends of the waveguide have been short-circuited with two brass plates. The cavity thus obtained can be put in resonance in many ways. We are interested in those modes which are related to the longitudinal propagation.

Moreover, expressing (2) in terms of wavelenghts we can obtain the well known equation

$$(7) \qquad 1/\lambda_c^2 = 1/\lambda^2 - 1/\lambda_g^2$$

where λ_g is the guide wavelenght.

Measuring the resonant frequencies and using (7) we can calculate the parallelogram shaped guide cut-off frequencies.

The cavity was coupled to the signal generator and to the measuring device with very small loops that didn't appreciably affected the guide characteristics.

The signal, after demodulation, was displayed, together with the frequency marks, on the screen of a Polyskop IV Rhode & Schwarz, with the sweep sinchronized with the signal generator.

The inner design dimensions of the rectangular cavity resonator were of 400, 564 and 700 mm and the mechanical realization introduced errors of only few millimeters, that however affected the parallelism of corresponding sides.

The TE_{10} propagation mode corresponds to the resonance TE_{101} and, as is expected, the resonant frequency decreases when the angle α decreases. This is the dominant mode for the parallelogram waveguide.

The TE_{01} corresponds to the resonance TE_{011}.

For α = 45° the measured frequency is 564.8 ± 0.25 MHz, while the one calculated with (6) and (7) is 564.3 ± 1.8 MHz.

The errors are large because of the poor parallelism, but the separation with further resonances is significant and so the previous hypothesis about the pattern modification of the electromagnetic fields seems to be very probable.

In the fig. 4, 5, 6 there are graphs of the cut-off wavelenghts, normalized to the corresponding ones of the rectangular guide, shown for different ratios of the sides in the cross section of the waveguide, versus the angle α, for the modes derived from TE_{10}, TE_{01} and TE_{11}.

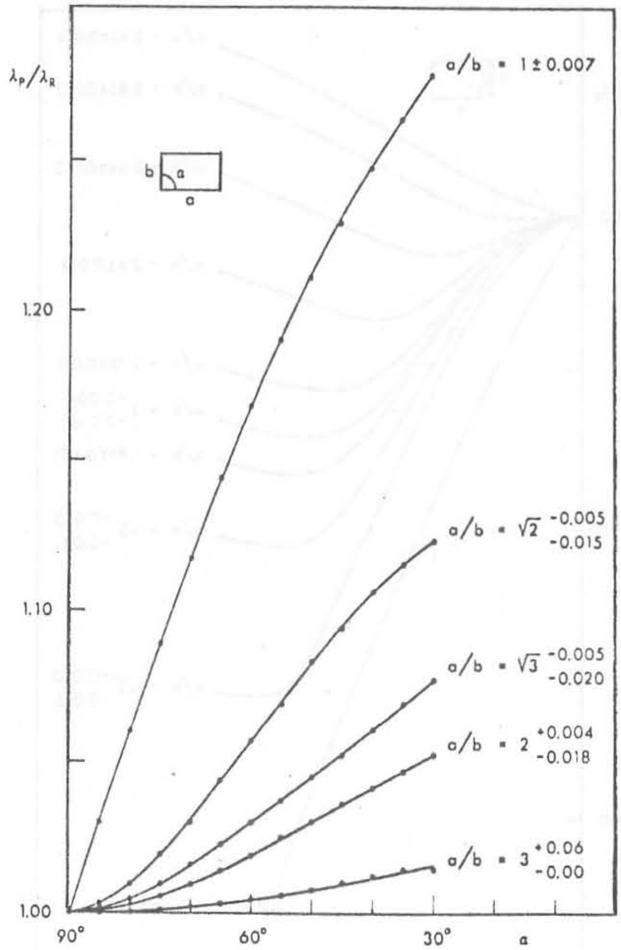

Fig. 4 - TE_{10} derived cut-off wavelenghts λ_P of the parallelogram waveguide, normalized to the cut-off wavelenghts λ_R of the rectangular guide for various ratios of the sides of the cross-section. The dots are experimental points. The error is ± 0.5°; ± 0.005 .

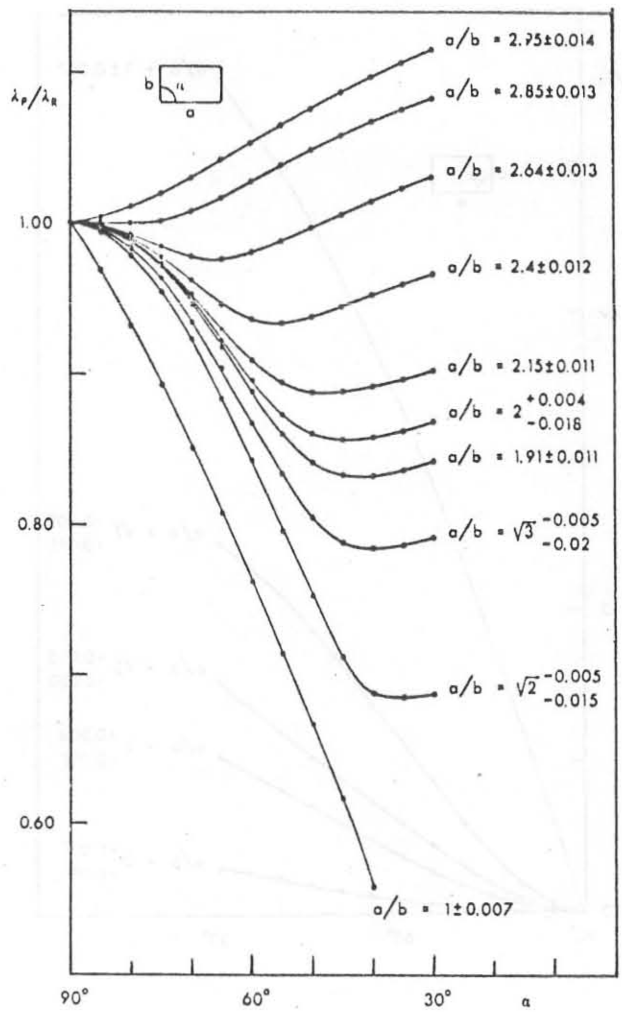

Fig. 5 - TE_{01} derived cut-off wavelenghts λ_P of the parallelogram guide, normalized to the cut-off wavelenght λ_R for various ratios of the sides of the cross section. The dots are experimental points. The error is $\pm 0.5°$; ± 0.005 .

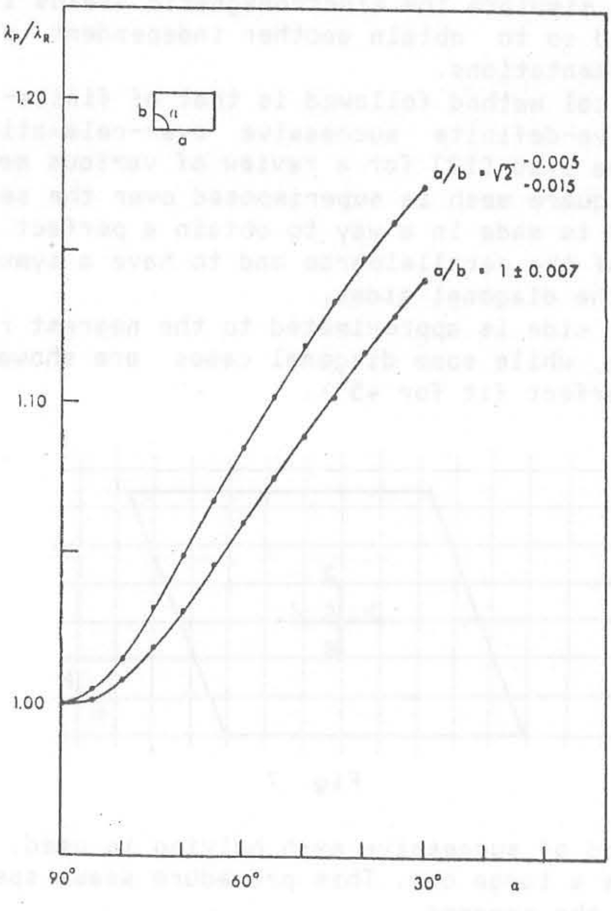

Fig. 6 - TE_{11} derived cut-off wavelenghts λ_P of the parallelogram guide, normalized to the cut-off wavelenght λ_R for two ratios of the sides of the cross section. The dots are experimental points. The error is $\pm 0.5°$; ± 0.005 .

NUMERICAL SOLUTION

A computer program written in FORTRAN on a VAX/11-750 has been made to simulate the electromagnetic fields into the waveguide, and so to obtain another independent proof of the theoric argumentations.

The numerical method followed is that of finite-difference, with positive-definite successive over-relaxation (PDSOR) [6], [9]; see also [12] for a review of various methods.

First a square mesh is superimposed over the section as in fig. 7. This is made in a way to obtain a perfect fit on the lower side of the parallelogram and to have a symmetrical situation on the diagonal sides.

The upper side is approximated to the nearest row of nodes of the mesh, while some diagonal cases are showed in fig. 8 (note the perfect fit for 45°).

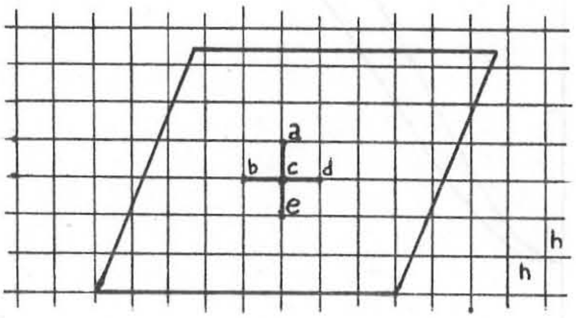

Fig. 7

The method of successive mesh halving is used, so the initial mesh is a large one. This procedure seems speed the convergence of the process.

Referring to fig. 7, equation (1) written in his finite-difference form becomes

$$(8) \qquad (4-\lambda)\varphi_c - \varphi_a - \varphi_b - \varphi_d - \varphi_e = 0$$

having put

$$(9) \qquad \lambda = (h\, k_c)^2$$

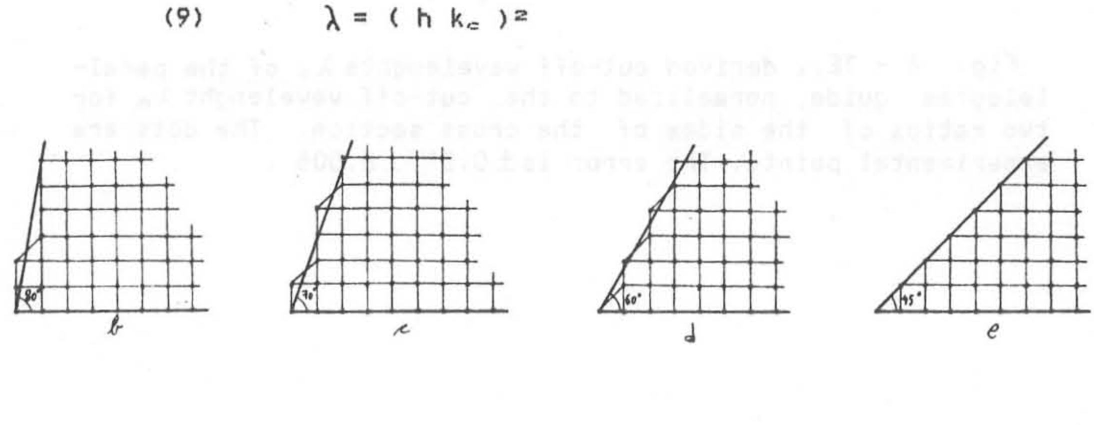

Fig. 8

(8) is often referred to as the five-point operator equation, because in it appear the central node and the four adjacent ones.

It is clear that this equation represents an eigenvalue problem of type

$$(10) \qquad (A - \lambda I)\Phi = 0$$

where Φ is the column vector formed by the values of φ_i at the various nodes.

Let us put

$$(11) \qquad B = A - \lambda I$$

To solve (11) we use a direct standard method on a coarse mesh. In this manner we obtain an initial estimate of the eigenvalues and eigenvectors. At this point, (8) is applied subsequently to all nodes of the mesh for a small number of iterations with λ fixed, then we use the actual value of Φ to compute a new value of λ through the formula (see [7] pp. 74-75)

$$(12) \qquad \lambda^{(r+1)} = (\Phi^{(r)T} A \, \Phi^{(r)})/(\Phi^{(r)T} \Phi^{(r)})$$

where r is the progressive iteration number and T indicate the transpose of a matrix.

This process is repeated to obtain a new estimate of Φ and so on.

A theorem [8] ensures correct convergence of this method if and only if B is a positive semidefinite matrix.

So, in general, successful iterations of (11) are guaranteed only for the fundamental mode, because for higher order modes B isn't a positive semidefinite matrix yet (see [9] p. 427).

To avoid this, a new matrix

$$(13) \qquad C = B^T B$$

is defined.

Since

$$\det(C) = \det(B^T) \det(B) = (\det(B))^2$$

the following equation

$$(14) \qquad C \, \Phi = 0$$

is satisfied by the same eigenvalues and eigenvectors that satisfy (11).

It is possible to demonstrate [10] that the symmetric matrix C is positive semidefinite for correct eigenvalues and positive definite elsewhere.

From the practical point of view, the reliability of using (14) instead of (11) arises from the fact that the rows of C can be generated one at a time, in the moment they are needed.

More exactly, as well explained in [10], the only nodes involved in computation of the coefficients c_{ij} are the central node and the twelve adjacent ones (fig. 9).

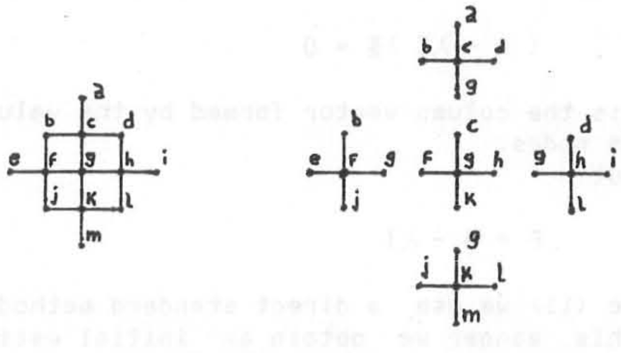

Fig. 9

Thus in this case we have

$$(15) \qquad c_{ga}\varphi_a + c_{gb}\varphi_b + \ldots + c_{gm}\varphi_m = 0$$

instead of (8).

The coefficients c_{rs} of the matrix C appearing in this equation are easily calculated from the coefficients of B, as illustrated in [10].

However, since we use the relaxation method to speed the convergence, equation (15) is not really used. Instead it is replaced by

$$(16) \qquad \varphi_g^{(r+1)} = (1-\omega)\varphi_g^{(r)} - \omega(c_{ga}\varphi_a^{(r+1)} + \ldots c_{gf}\varphi_f^{(r+1)} + c_{gh}\varphi_h^{(r)} + \ldots + c_{gm}\varphi_m^{(r)}) / c_{gg}$$

where ω is the accelerating factor that varies in the range 0 to 2.

In case $\omega = 1$ equation (16) reduces to (15). If $\omega < 1$ we speak of under-relaxation, that doesn't however take place in our case. So, because in general $1 < \omega < 2$, the method is called over-relaxation.

Equation (16) converges rapidly for an appropriate choice of the parameter ω, but doesn't exists an analytical way to find this value. So we performed various trials, after which we chose the procedure indicated by Carrè [11].

There are some controls to prevent the appearance of oscillations of the eigenvalues or eigenvectors around the solution; we have found good to put $\omega = 1$ for a few iterations when the solution shows some tendency to oscillate.

The process is terminated when the differences between successive estimates of λ and Φ, calculated respectively with (12) and with a computation of a term R called "residual" [10], are simultaneously smaller than prefixed constants.

Notice that the thirteen-point operator defined by (15) can be treated as composed by five operators of five-point type (fig. 9). So the boundary conditions problem reduces to that of five-point operators.

In our case the manners in which such operators can stand with respect of the borders are showed in fig. 10.

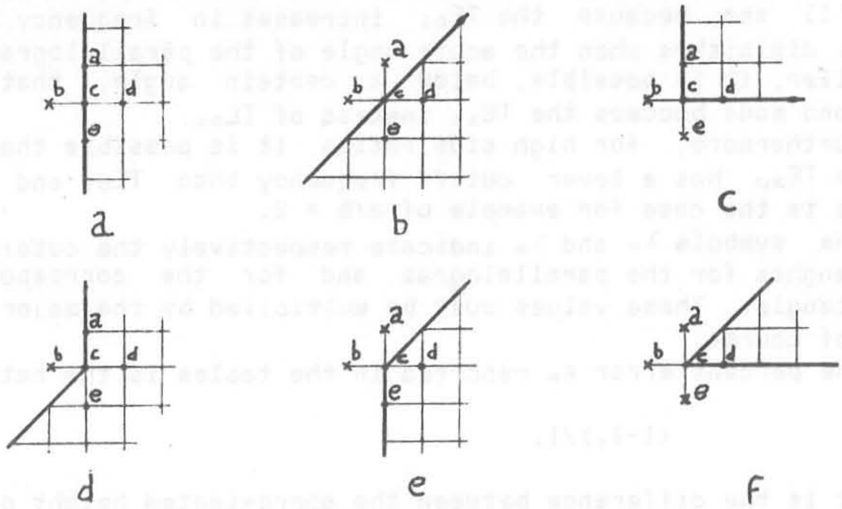

Fig. 10

For each case the introduction of condition (4) in (8) has been treated by the following equations (in order a to f):

$$(4 - \lambda)\varphi_c - \varphi_a - 2\varphi_d - \varphi_e = 0$$

$$(4 - \lambda)\varphi_c - 2\varphi_d - 2\varphi_e = 0$$

$$(4 - \lambda)\varphi_c - 2\varphi_a - 2\varphi_d = 0$$

$$(4 - \lambda)\varphi_c - \varphi_a - \varphi_d - 2\varphi_e = 0$$

$$(4 - \lambda)\varphi_c - 3\varphi_d - \varphi_e = 0$$

$$(2 - \lambda)\varphi_c - 2\varphi_d = 0$$

The criterion used to obtain these equations is the following: for each point outside the border (marked by a 'x' in fig. 10) we have defined its image-point, i.e. the point symmetrical with respect to the border.

For instance, in case b, the image-point of point b is e; in case e, point d is the image-point of both points a and b.

Hence, the boundary condition (4) is simulated assigning to the external point a value equal to its image-point.

Notice that in case f, the laplacian operator reduces only to the x-component.

If we had considered the TM modes, the condition (3) would have been much easier to simulate.

In fact in this case it is only necessary to put equal to zero all the boundary nodes.

Implementing these ideas in the computer program we have obtained the following results.

NUMERICAL RESULTS

The following tables contain the data obtained from the program for various angles and for three ratios between sides.

These data refer to the fundamental mode (TE_{10}) and the two modes immediately following, i.e. TE_{01} and TE_{11}. As you'll see, because the TE_{01} increases in frequency while TE_{11} diminishes when the acute angle of the parallelogram get smaller, it is possible, below a certain angle, that the second mode becomes the TE_{11} instead of TE_{01}.

Furthermore, for high side ratios, it is possible that the mode TE_{20} has a lower cutoff frequency than TE_{01} and TE_{11}; this is the case for example of a/b = 2.

The symbols λ_P and λ_R indicate respectively the cutoff wavelenghts for the parallelogram and for the corresponding rectangle. These values must be multiplied by the major side a, of course.

The percent error ε_R reported in the tables is the ratio

$$(l-l_t)/l_t$$

that is the difference between the approximated height of the parallelogram 'l' and the true height 'l_t', divided by l_t itself. Naturally, ε_R greater than zero means an excess approximation of the height and conversely.

This error alters above all the modes TE_{01} and TE_{11}. His influence can be estimated through the following considerations: if, referring for instance to the case $a/b = \sqrt{2}$, we calculate the cutoff frequency of a rectangular guide with sides 'a' and '$a(1+\varepsilon_R)/\sqrt{2}$', we find the result 1.4286a for the cutoff wavelenght TE_{01}; this number is not much close to the theoric result ($\sqrt{2}$); note however that it is very good when compared with the value in the table 2.

		TE_{10}		TE_{01}		TE_{11}	
$\alpha°$	ε_R (%)	λ_P	λ_P/λ_R	λ_P	λ_P/λ_R	λ_P	λ_P/λ_R
90	0.00	1.99995	0.99998	1.99995	0.99998	1.41418	0.99998
85	0.38	2.07294	1.03647	1.92745	0.96372	1.41631	1.00148
80	1.54	2.15371	1.07690	1.85900	0.92950	1.43602	1.01542
75	3.53	2.20385	1.10192	1.79228	0.89614	1.44288	1.02027
70	-1.18	2.25290	1.12645	1.66565	0.83283	1.45583	1.02943
65	0.31	2.32848	1.16424	1.58823	0.79412	1.48863	1.05262
60	-1.03	2.36243	1.18121	1.48657	0.74328	1.49767	1.05902
55	-0.11	2.41373	1.20686	1.39546	0.69773	1.52628	1.07924
50	0.42	2.44769	1.22385	1.29985	0.64992	1.54562	1.09292
45	1.02	2.47868	1.23934	1.19901	0.59951	1.56486	1.10652
40	0.01	2.18042	1.09021	1.01236	0.50618	1.42622	1.00849

TABLE 1 - Numerical results for various angles and modes, and for a ratio a/b=1.

		TE 10		TE 01		TE 11	
$\alpha°$	ε_R (%)	λ_P	λ_P/λ_R	λ_P	λ_P/λ_R	λ_P	λ_P/λ_R
90	1.02	1.99995	0.99997	1.42854	1.01014	1.16245	1.00671
85	1.40	2.00341	1.00171	1.42546	1.00795	1.16728	1.01089
80	-0.58	2.01799	1.00899	1.37241	0.97045	1.17153	1.01458
75	1.36	2.04135	1.02068	1.36431	0.96471	1.20562	1.04410
70	0.33	2.06806	1.03403	1.30179	0.92051	1.22278	1.05896
65	0.31	2.09861	1.04930	1.24833	0.88270	1.24440	1.07768
60	0.49	2.12536	1.06268	1.19303	0.84360	1.26209	1.09300
55	0.71	2.15197	1.07599	1.12503	0.79552	1.28689	1.11448
50	-0.59	2.15956	1.07978	1.04855	0.74144	1.29211	1.11900
45	0.00	2.18453	1.09226	0.99905	0.70643	1.30913	1.13374
40	0.01	2.12521	1.06261	0.97184	0.68719	1.30528	1.13041

TABLE 2 - Numerical results for various angles and modes, and for a ratio $a/b=\sqrt{2}$ between sides.

		TE 10		TE 20	TE 01	TE 11	
$\alpha°$	ε_R (%)	λ_P	λ_P/λ_R	λ_P	λ_P	λ_P	λ_P/λ_R
90	0.00	1.99994	0.99997	0.99999	0.99999	0.89441	0.99998
85	0.38	2.00172	1.00086	1.00086	0.99895	0.88904	0.99398
80	1.54	2.00667	1.00333	1.02168	0.99965	0.87691	0.98042
75	3.53	2.01448	1.00724	1.04722	0.96248	0.85976	0.96124
70	-1.77	2.02249	1.01124	1.05549	0.92834	0.80462	0.89959
65	0.31	2.03731	1.01866	1.08173	0.91899	0.78236	0.87471
60	-1.03	2.04360	1.02180	1.09287	0.88123	0.74511	0.83306
55	1.73	2.05818	1.02909	1.11620	0.87548	0.72410	0.80957
50	0.42	2.05996	1.02998	1.12409	0.85197	0.69225	0.77396
45	1.02	2.06370	1.03185	1.13748	0.85189	0.67292	0.75235
40	3.71	1.99710	0.99855	1.12760	0.85263	0.63295	0.70766

TABLE 3 - Numerical results for various angles and modes, and for a ratio a/b=2. The modes TE_{20} and TE_{01} have λ_R equal to one. The TE_{21}, not reported here, below 60° becomes the fourth mode instead of TE_{11} that shows now a decrease of his λ_P when α diminishes.

A comparison between numerical and experimental data can be done through the following diagrams. Here the small circles represent the computed results and the curves are those previously seen in figg. 4, 5 and 6.

Apart from the height imprecision, there is another source of error. In fact below 45° the boundary conditions approximation can give rise to an erratic behaviour of the fields near the acute angles. This affects mostly the TE_{10} and TE_{11} modes. To avoid this it would be necessary to introduce much more complex approximations of (4); see for instance [13].

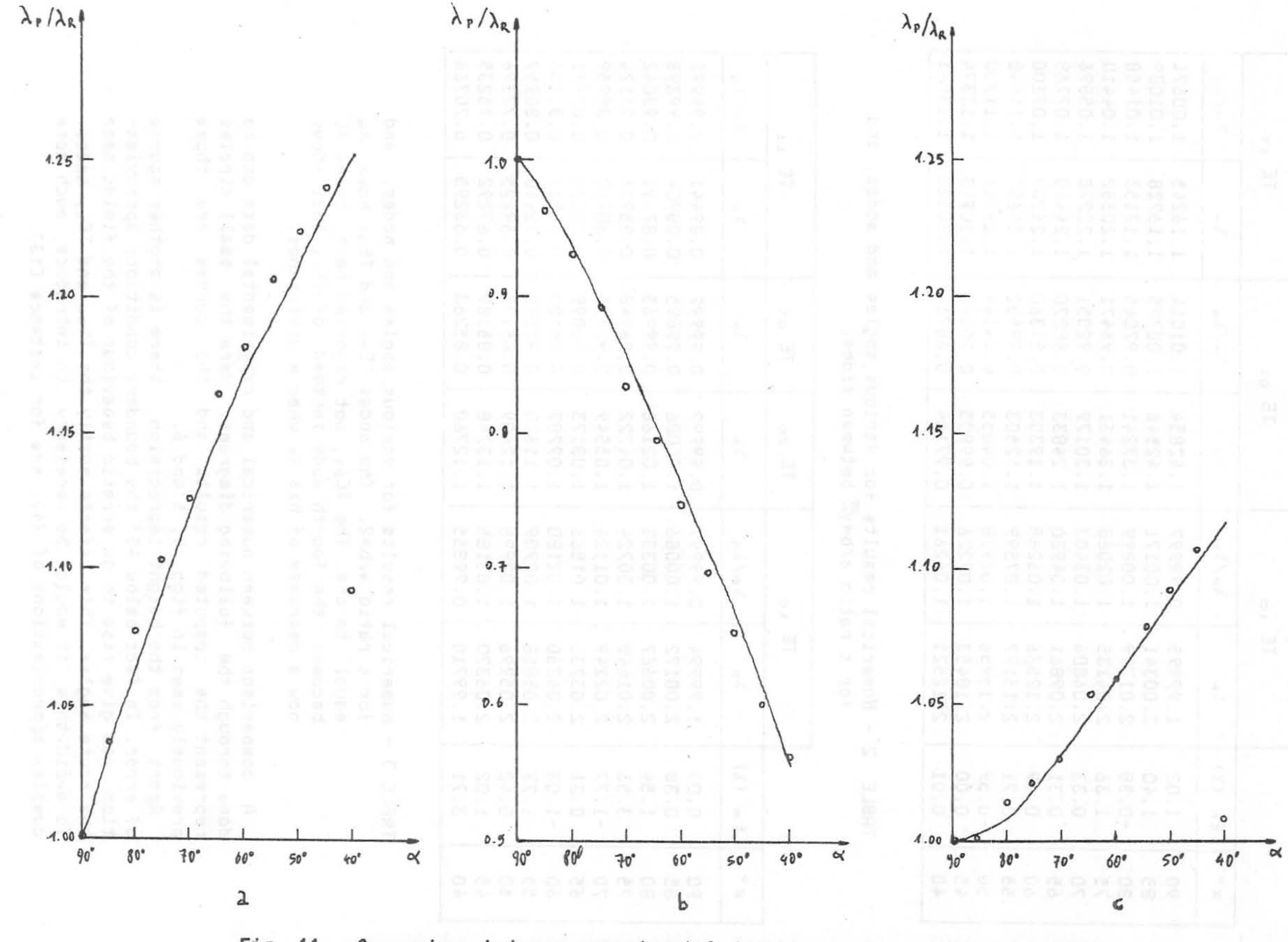

Fig. 11 - Comparison between experimental (continuous curves) and computed results (circles) for a ratio a/b = 1; a: TE_{10}, b: TE_{01}, c: TE_{11}.

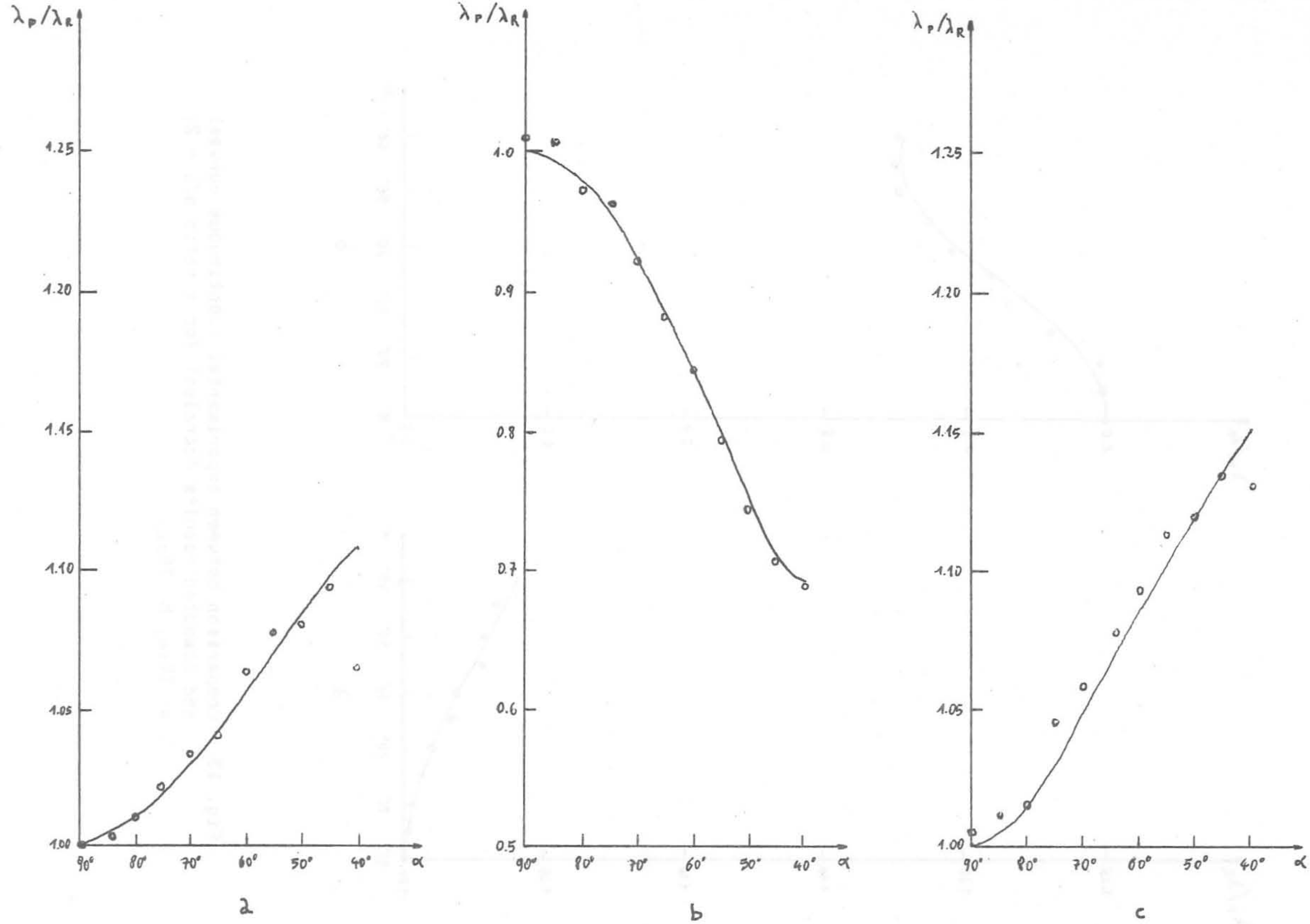

Fig. 12 - Comparison between experimental (continuous curves) and computed results (circles) for a ratio $a/b = \sqrt{2}$; a: TE_{10}, b: TE_{01}, c: TE_{11}.

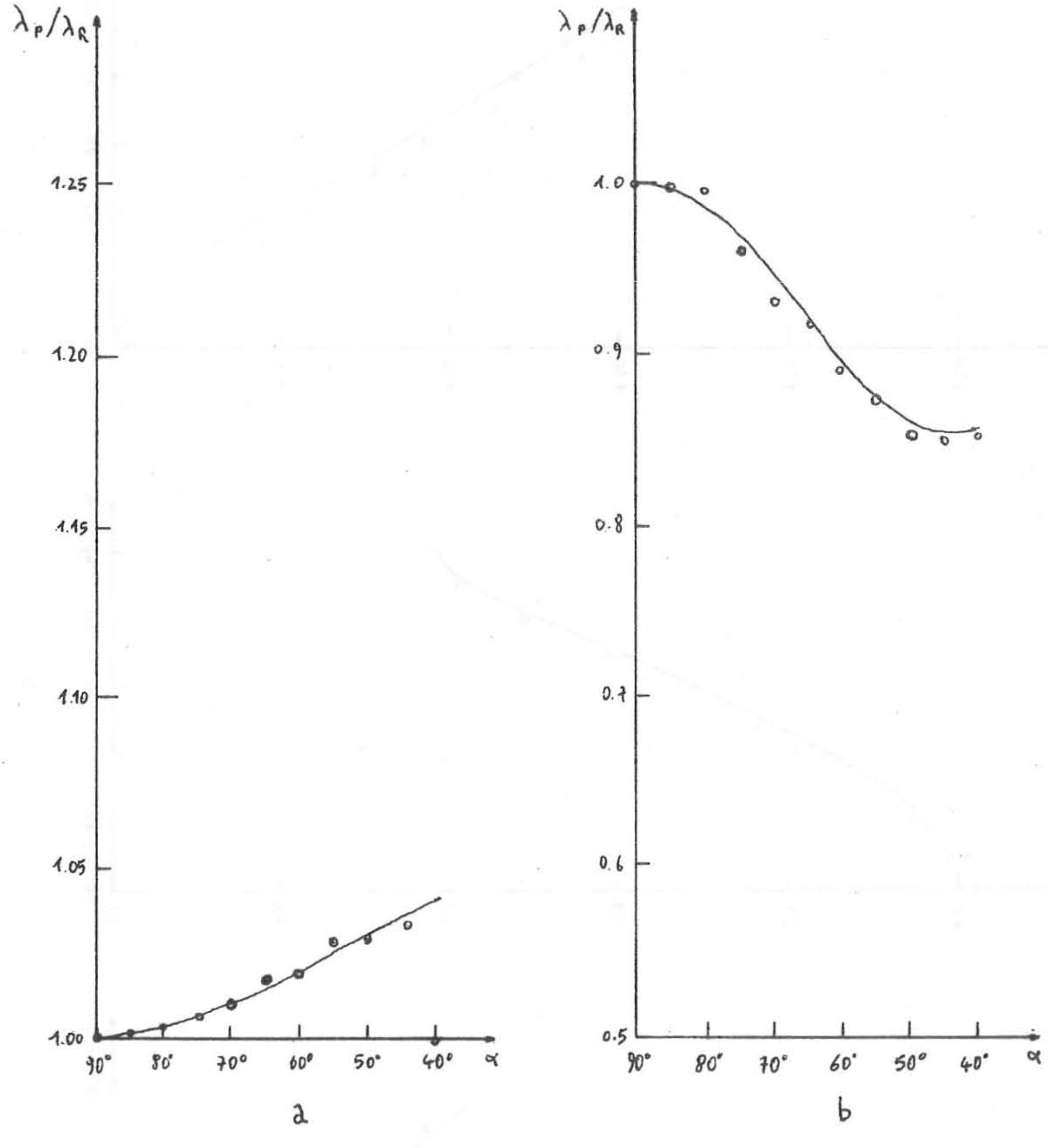

Fig. 13 - Comparison between experimental (continuous curves) and computed results (circles) for a ratio a/b = 2; a: TE_{10}, b: TE_{01}.

Finally the graphics below show the behaviour of the transverse electric field for various cross-sections.
Notice that some graphs are composed by dotted lines too. In this case the continuous curves represent a field going toward the top of the parallelogram, while dotted lines are those in which the field goes toward the bottom.
In other graphs there are some arrows to indicate the direction in which the lines flow.

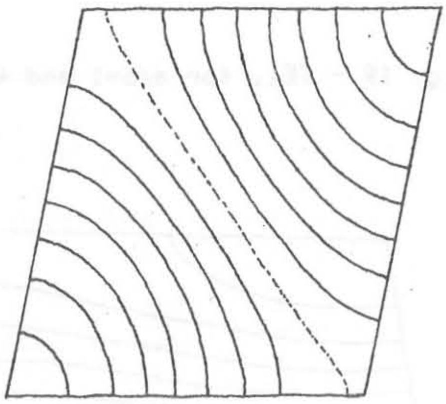

Fig. 14 - TE_{10} for a/b=1 and 80°

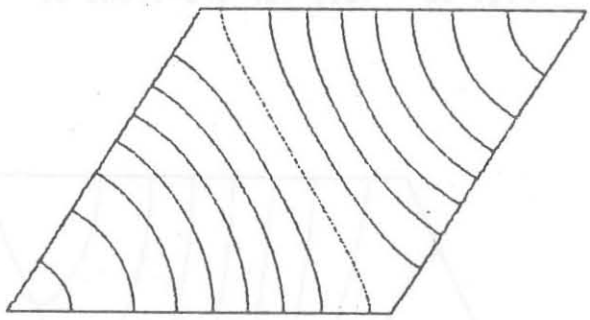

Fig. 15 - TE_{10} for a/b=1 and 60°

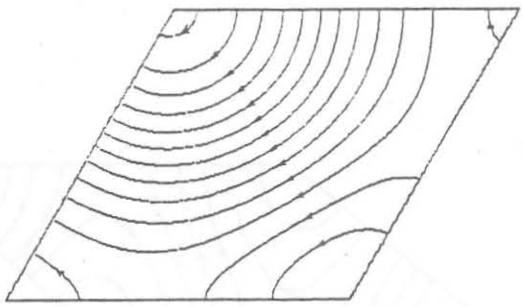

Fig. 16 - TE_{01} for a/b=1 and 60°

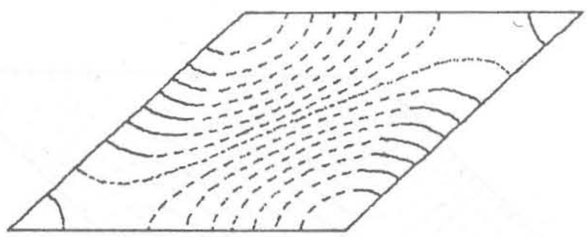

Fig. 17 - TE_{01} for a/b=1 and 45°

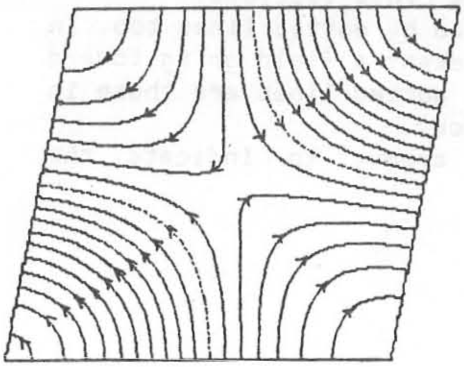

Fig. 18 - TE_{11} for a/b=1 and 80°

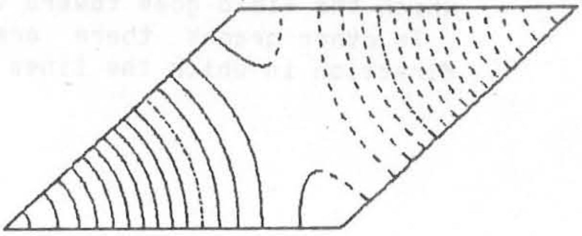

Fig. 19 - TE_{11} for a/b=1 and 45°

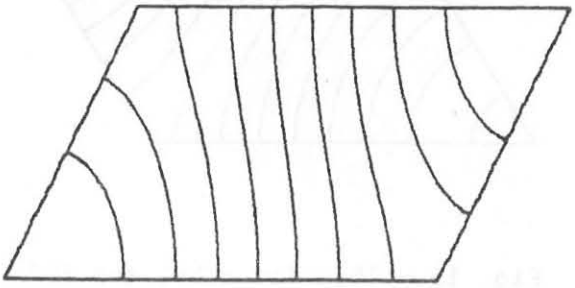

Fig. 20 - TE_{10} for $a/b=\sqrt{2}$ and 65°

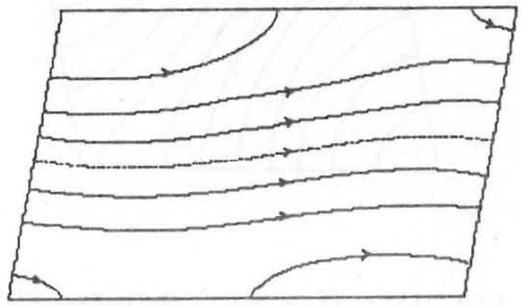

Fig. 21 - TE_{01} for $a/b=\sqrt{2}$ and 80°

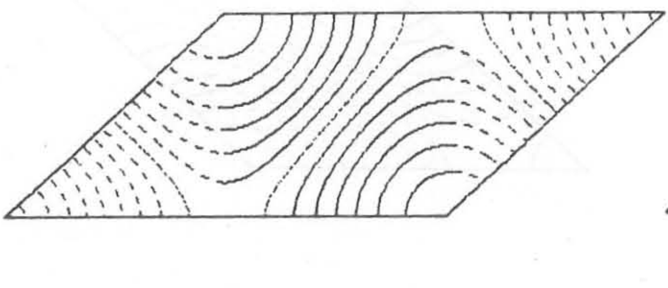

Fig. 22 - TE_{01} for $a/b=\sqrt{2}$ and 45°

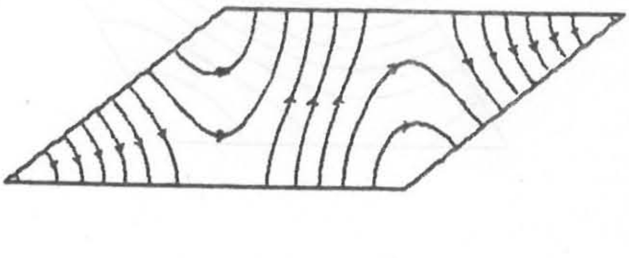

Fig. 23 - TE_{01} for $a/b=\sqrt{2}$ and 40°

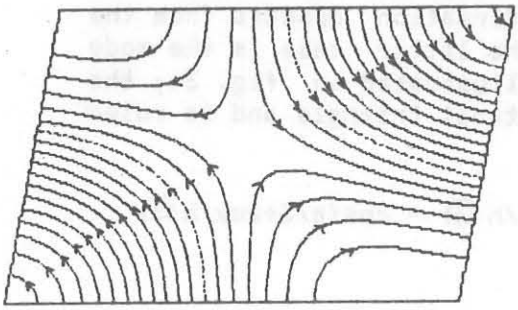

Fig. 24 - TE_{11} for $a/b=\sqrt{2}$ and 80°

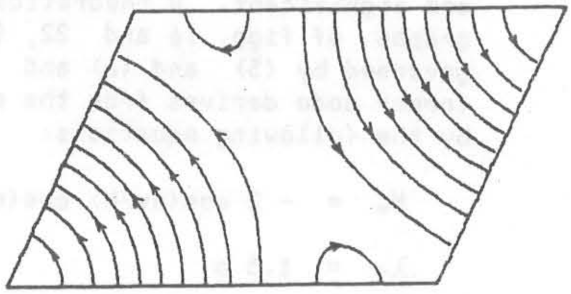

Fig. 25 - TE_{11} for $a/b=\sqrt{2}$ and 65°

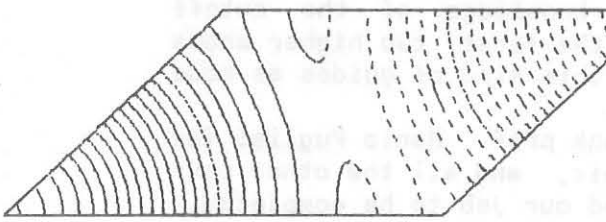

Fig. 26 - TE_{11} for $a/b=\sqrt{2}$ and 45°

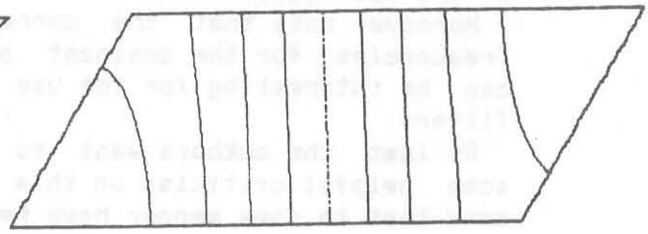

Fig. 27 - TE_{10} for $a/b=2$ and 60°

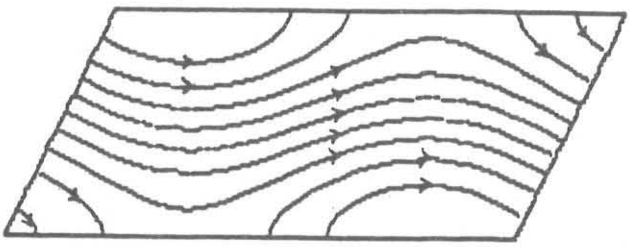

Fig. 28 - TE_{01} for $a/b=2$ and 65°

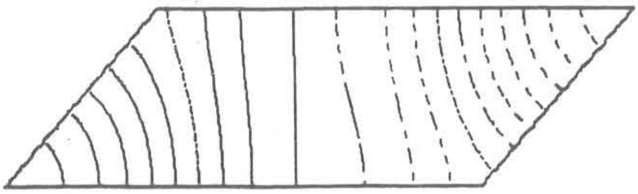

Fig. 29 - TE_{20} for $a/b=2$ and 50°

CONCLUSIONS

In spite of some occasional problem, the results obtained are significant. A theoretical confirmation appears from the graphs of figg. 16 and 22, too. The latter case is the mode governed by (5) and (6) and yet illustrated in fig. 3a; the former mode derives from the equilateral triangle and is ruled by the following equations:

$$H_z = -2\cos(\pi y/h)\cos(\pi/3-\pi x/h\sqrt{3}) - \cos(\pi/3+2\pi x/h\sqrt{3})$$

$$\lambda_c = 1.5\ a$$

where h is the height of the parallelogram.

So we can tell to have achieved in this work two principal results: first, both the experiments and the numerical iterations have revealed the existence of a previously unknown dominant mode; now remains opened the problem to find analytical solutions in terms of elementary functions for it, and even for a generic mode, if possible.

Then we've got an idea about the fields pattern inside the waveguide, and how it changes varying the acute angle of the parallelogram. At this purpose very interesting is the shape of the TE_{11} mode.

Moreover note that the correct knowledge of the cutoff frequencies for the dominant and the first two higher modes can be interesting for the use of this kind of guides as mode filters.

At last the authors want to thank prof. Mario Puglisi for some helpful criticism on this topic, and all the other persons that in some manner have helped our job to be completed.

REFERENCES

[1] see for instance: A.F. Harvey, "Microwave engineering", Academic Press, London and New York, 1963;

[2] Swift W.B. and Higgins T.J., "Electromagnetic propagation through waveguide of rhombic cross-section", Proc. Nat. Electronics Conference, Chicago, 1952, 8, p. 247;

[3] Schelkunoff S.A., "Electromagnetic waves", Van Nostrand, New York, 1943, p. 393;

[4] Malvano R., "Metal waveguides with parallelogram cross-section", Nuovo Cimento, 1949, 6, p. 265;

[5] Schelkunoff S.A., op. cit., p. 395;

[6] Beaubien M.J. and Wexler A., "Unequal-arm finite-difference operators in the positive-definite successive over-relaxation (PDSOR) algorithm", IEEE Trans. on Microwave Theory and Techniques, December 1970, pp. 1132÷1134;

[7] Fox L., "Numerical solution of ordinary and partial differential equations", Pergamon Press, Oxford, 1962;

[8] Forsythe G.F. and Wasow W.R., "Finite-difference methods for partial differential equations", Wiley, New York, 1967, pp. 375-376;

[9] Wexler A., "Computation of electromagnetic fields', IEEE Trans. on Microwave Theory and Techniques, August 1969, pp. 416÷439;

[10] Beaubien M.J. and Wexler A., "An accurate finite-difference method for higher order waveguide modes", IEEE Trans. on Microwave Theory and Techniques, December 1968, pp. 1007÷1017;

[11] Carrè B.A., "The determination of the optimum accelerating factor for successive over-relaxation", Computer Journal, vol. 4, 1961, pp. 73÷78;

[12] Fook Loy Ng, "Tabulation of methods for the numerical solution of the hollow waveguide problem", IEEE Trans. on Microwave Theory and Techniques, March 1974, pp. 322÷329;

[13] Mur G., "The modeling of singularities in the finite difference approximation of the time-domain electromagnetic-field equations", IEEE Trans. on Microwave Theory and Techniques, October 1981, pp. 1073÷1077;